Multidimensional Heteronuclear Correlation Spectroscopy of a Uniformly ^{15}N- and ^{13}C-Labeled Peptide Crystal: Toward Spectral Resolution, Assignment, and Structure Determination of Oriented Molecules in Solid-State NMR

Yoshitaka Ishii and Robert Tycko*

Contribution from the Laboratory of Chemical Physics, National Institute of Diabetes and Digestive and Kidney Diseases, National Institutes of Health, Bethesda, Maryland 20892-0520

Received May 10, 1999

Abstract: New one-, two-, and three-dimensional solid-state NMR spectroscopic methods designed for structural studies of uniformly ^{15}N- and ^{13}C-labeled peptides and proteins in oriented samples are described. These methods provide a means of obtaining resolved spectra, sequential resonance assignments, and structural constraints. Experimental results for model single-crystal peptides and amino acids demonstrate that high-resolution one-dimensional ^{13}C spectra can be obtained for signals from carbonyl or carboxyl (^{13}CO) carbons in uniformly labeled samples by applying phase-modulated selective homonuclear (PSH) decoupling at aliphatic carbon resonances, in addition to heteronuclear proton and ^{15}N decoupling. ^{13}C-detected two-dimensional ^{15}N/^{13}C chemical shift correlation spectroscopy is made possible by a combination of PSH decoupling and broadband heteronuclear polarization transfer sequences such as WALTZ-5 cross-polarization. Experimental two-dimensional spectra of uniformly ^{15}N- and ^{13}C-labeled AlaGlyGly crystals show that resolution and sequential assignment of ^{13}CO and ^{15}N NMR signals is possible. Comparisons of experimental spectra and simulations verify the assignments and the accuracy of structural information contained in the two-dimensional spectra in the form of the orientation-dependent ^{13}CO and ^{15}N chemical shifts. ^{13}C-detected three-dimensional spectroscopy is also demonstrated by adding a ^{1}H−^{15}N dipolar dimension to the two-dimensional methods. Results of experiments at fields of 9.39 and 17.6 T (400 and 750 MHz proton NMR frequencies) are reported. Motivations for uniform labeling and ^{13}C detection in oriented systems and implications for future structural studies of oriented proteins are discussed.

Introduction

Recent advances in solid-state NMR spectroscopy have made it a powerful tool for obtaining structural information such as internuclear distances[1−15] and dihedral angles[16−25] in solids,[26,27] liquid crystals,[28] and frozen solutions.[29,30] Applications to biological macromolecules have attracted much attention because solid-state NMR provides accurate structural parameters, information about structural distributions,[29,31] and long-range distance constraints even for proteins that cannot be studied by other methods because of their size, noncrystallinity, or other factors.[26,30,32−35] Until recently, structural information obtained

(1) Raleigh, D. P.; Levitt, M. H.; Griffin, R. G. *Chem. Phys. Lett.* **1988**, *146*, 71−76.
(2) Gullion, T.; Schaefer, J. *Adv. Magn. Reson.* **1989**, *13*, 57−83.
(3) Engelsberg, M.; Yannoni, C. S. *J. Magn. Reson.* **1990**, *88*, 393−400.
(4) Tycko, R.; Dabbagh, G. *Chem. Phys. Lett.* **1990**, *173*, 461−465.
(5) Gullion, T.; Vega, S. *Chem. Phys. Lett.* **1992**, *194*, 423−428.
(6) Fujiwara, T.; Ramamoorthy, A.; Nagayama, K.; Hioka, K.; Fujito, T. *Chem. Phys. Lett.* **1993**, *212*, 81−84.
(7) Baldus, M.; Tomaselli, M.; Meier, B. H.; Ernst, R. R. *Chem. Phys. Lett.* **1994**, *230*, 329−336.
(8) Ishii, Y.; Terao, T. *J. Magn. Reson. A* **1995**, *115*, 116−118.
(9) Lee, Y. K.; Kurur, N. D.; Helmle, M.; Johannessen, O. G.; Nielsen, N. C.; Levitt, M. H. *Chem. Phys. Lett.* **1995**, *242*, 304−309.
(10) Gregory, D. M.; Mitchell, D. J.; Stringer, J. A.; Kiihne, S.; Shiels, J. C.; Callahan, J.; Mehta, M. A.; Drobny, G. P. *Chem. Phys. Lett.* **1995**, *246*, 654−663.
(11) Hirao, K.; Ishii, Y.; Terao, T.; Kishimoto, Y.; Miyatake, T.; Ikariya, T.; Noyori, R. *Macromolecules* **1998**, *31*, 3405−3408.
(12) Bennett, A. E.; Rienstra, C. M.; Griffiths, J. M.; Zhen, W. G.; Lansbury, P. T.; Griffin, R. G. *J. Chem. Phys.* **1998**, *108*, 9463−9479.
(13) Bennett, A. E.; Weliky, D. P.; Tycko, R. *J. Am. Chem. Soc.* **1998**, *120*, 4897−4898.
(14) Hohwy, M.; Jakobsen, H. J.; Eden, M.; Levitt, M. H.; Nielsen, N. C. *J. Chem. Phys.* **1998**, *108*, 2686−2694.
(15) Nishimura, K.; Naito, A.; Tuzi, S.; Saito, H.; Hashimoto, C.; Aida, M. *J. Phys. Chem. B* **1998**, *102*, 7476−7483.
(16) Weliky, D. P.; Dabbagh, G.; Tycko, R. *J. Magn. Reson. A* **1993**, *104*, 10−16.
(17) Tomita, Y.; O'Connor, J.; McDermott, A. *J. Am. Chem. Soc.* **1994**, *116*, 8766−8771.
(18) Ishii, Y.; Terao, T.; Kainosho, M. *Chem. Phys. Lett.* **1996**, *256*, 133−140.
(19) Schmidt-Rhor, K. *Macromolecules* **1996**, *29*, 3975−3981.
(20) Weliky, D. P.; Tycko, R. *J. Am. Chem. Soc.* **1996**, *118*, 8487−8488.
(21) Feng, X.; Lee, Y. K.; Sandstrom, D.; Eden, M.; Maisel, H.; Sebald, A.; Levitt, M. H. *Chem. Phys. Lett.* **1996**, *257*, 314−320.
(22) Fujiwara, T.; Shimomura, T.; Akutsu, H. *J. Magn. Reson.* **1997**, *124*, 147−153.
(23) Ishii, Y.; Hirao, K.; Terao, T.; Terauchi, T.; Oba, M.; Nishiyama, K.; Kainosho, M. *Solid State Nucl. Magn.* **1998**, *11*, 169−175.
(24) Hong, M.; Gross, J. D.; Griffin, R. G. *J. Phys. Chem. B* **1997**, *101*, 5869−5874.
(25) Costa, P. R.; Gross, J. D.; Hong, M.; Griffin, R. G. *Chem. Phys. Lett.* **1997**, *280*, 95−103.
(26) Griffin, R. G. *Nat. Struct Biol.* **1998**, *5*, 508−512.
(27) Terao, T. *J. Mol. Struct.* **1998**, *441*, 283−294.
(28) Kimura, A.; Kuni, N.; Fujiwara, H. *J. Am. Chem. Soc.* **1997**, *119*, 4719−4725.
(29) Long, H. W.; Tycko, R. *J. Am. Chem. Soc.* **1998**, *120*, 7039−7048.
(30) Weliky, D. P.; Bennett, A. E.; Zvi, A.; Anglister, J.; Steinbach, P. J.; Tycko, R. *Nat. Struct Biol.* **1999**, *6*, 141−145.
(31) Schmidt-Rohr, K.; Spiess, H. W. *Multidimensional solid-state NMR and polymers*; Academic Press Inc.: San Diego, 1994.

10.1021/ja9915753 CCC: $19.00
Published on Web 02/02/2000

by solid-state NMR has been limited to local structural features of biopolymers that are selectively isotopically labeled.[26,27,29,30,32−34] The determination of global structures of uniformly isotopically labeled proteins by solid-state NMR remains a challenging problem because of the limited resolution in solid-state NMR spectra (compared to liquid-state NMR spectra) and the early developmental stage of methods for resonance assignment and the extraction of structural constraints from multidimensional solid-state NMR spectra of uniformly labeled, high molecular weight samples. So far, two major approaches have been pursued. One approach is to use magic angle spinning[36] (MAS) to obtain high-resolution spectra of unoriented proteins (e.g., frozen protein solutions, unoriented membrane-associated proteins, and lyophilized, precipitated, fibrous, or polycrystalline proteins). Advantages of the MAS approach include its broad range of applicability, the ability to switch homonuclear and heteronuclear dipole−dipole couplings on and off with MAS recoupling sequences,[1,4−10,37] and the availability of isotropic chemical shift information in MAS spectra, which may facilitate resonance assignment. Although considerable progress is being made,[38−42] current challenges within the MAS approach include the limited resolution in isotropic chemical shift spectra[43] and uncertainties regarding the extraction of structural constraints from MAS spectra of uniformly labeled molecules.

The second approach to global structure determination in uniformly labeled proteins is to study oriented systems, i.e., systems with at least uniaxial order, aligned with the external magnetic field either mechanically[44−48] or magnetically.[49−52] Solid-state NMR spectra of well-oriented proteins[53] can exhibit better resolution than MAS spectra because the ranges of ^{13}C and ^{15}N NMR frequencies can be 100−200 ppm due to the chemical shift anisotropies (CSA), particularly for carbonyl ^{13}C and amide ^{15}N sites. In addition, measurements of anisotropic chemical shifts, dipole−dipole splittings, and quadrupole splittings in spectra of oriented systems provide structural constraints in a direct manner[54,55] through the well-known dependences of these parameters on the orientations of chemical functional groups relative to the external field. Finally, the approach of studying oriented systems is of particular relevance to integral membrane proteins and other membrane-associated proteins because of the ability to orient biological model membranes mechanically[44−48] or magnetically.[49−52] Applications of solid-state NMR to membrane proteins are especially important due to the difficulty of crystallizing membrane proteins for diffraction measurements and the long rotational correlation times for membrane proteins in true membrane environments, which currently preclude liquid-state NMR measurements. For these reasons, we focus on the development of methods for oriented proteins in this paper.

Several groups have pursued solid-state NMR measurements on oriented peptides and proteins.[44,45,48,49,56−58] For example, Cross and co-workers[45,57,59] have developed a detailed molecular structure of gramicidin-A, a 15-residue channel-forming peptide, in phospholipid bilayers by measuring a series of anisotropic ^{15}N chemical shifts of amide nitrogen, heteronuclear dipole−dipole couplings, and ^{2}H quadrupole splittings in mechanically oriented samples. For these studies, Cross and co-workers prepared a large series of gramicidin-A samples labeled at specific residues using solid-phase peptide synthesis[60] in order to make the spectral assignments and to overcome spectral overlaps. Other groups have also carried out measurements on specifically labeled synthetic[61,62] and expressed[63,64] membrane-bound peptides and proteins to determine the conformation or orientation relative to the membrane of the labeled segments.

Because it is generally impractical to synthesize or express a sufficiently large series of selectively labeled samples to determine the full structure of a protein in an oriented system, recent work, notably by Opella and co-workers,[53,65,66] has focused on the development and application of methods for resonance assignment and structure determination from multidimensional solid-state NMR spectra of uniformly labeled oriented proteins. The initial emphasis of this work was on uniformly ^{15}N-labeled proteins, with detection of ^{15}N NMR signals. Opella and co-workers have developed multidimensional PISEMA experiments[65,66] that enable the resolution of signals and the measurement and correlation of ^{1}H chemical shifts, $^{1}H-^{15}N$ dipole−dipole couplings, and ^{15}N chemical shifts. Although

(32) Hing, A. W.; Tjandra, N.; Cottam, P. F.; Schaefer, J.; Ho, C. *Biochemistry* **1994**, *33*, 8651−8661.
(33) Christensen, A. M.; Schaefer, J. *Biochemistry* **1993**, *32*, 2868−2873.
(34) Lansbury, P. T.; Costa, P. R.; Griffiths, J. M.; Simon, E. J.; Auger, M.; Halverson, K. J.; A., K. D.; Hendsch, Z. S.; Ashburn, T. T.; Spencer, R. G. S.; Tidor, B.; Griffin, R. G. *Nat. Struct. Biol.* **1995**, *2*, 990−998.
(35) Feng, X.; Verdegem, P. J. K.; Lee, Y. K.; Sandstorm, D.; Eden, M.; Bovee-Geurts, P.; de Grip, W. J.; Lugtenburg, J.; de Groot, H. M. J.; Levitt, M. H. *J. Am. Chem. Soc.* **1997**, *119*, 6853−6857.
(36) Andrew, E. R. *Nature* **1958**, *182*, 1659.
(37) Gullion, T.; Schaefer, J. *J. Magn. Reson.* **1989**, *81*, 196−200.
(38) Fujiwara, T.; Sugase, K.; Kainosho, M.; Ono, A.; Akutsu, H. *J. Am. Chem. Soc.* **1995**, *117*, 11351−11352.
(39) Boender, G. J.; Raap, J.; Prytulla, S.; Oschkinat, H.; Degroot, H. J. M. *Chem. Phys. Lett.* **1995**, *237*, 502−508.
(40) Nomura, K.; Takegoshi, K.; Terao, T.; Uchida, K.; Kainosho, M. *J. Am. Chem. Soc.* **1999**, *121*, 4064−4065.
(41) Hong, M. *J. Magn. Reson.* **1999**, *136*, 86−91.
(42) Rienstra, C. M.; Hatcher, M. E.; Mueller, L. J.; Sun, B. Q.; Fesik, S. W.; Griffin, R. G. *J. Am. Chem. Soc.* **1998**, *120*, 10602−10612.
(43) Tycko, R. *J. Biomol. NMR* **1996**, *8*, 239−251.
(44) Cornell, B. A.; Separovic, F.; Baldassi, A. J.; Smith, R. *Biophys. J.* **1998**, *53*, 67−76.
(45) Ketchem, R. R.; Hu, W.; Cross, T. A. *Science* **1993**, *261*, 1457−1460.
(46) Shon, k. J.; Kim, Y.; Colnago, L. A.; Opella, S. J. *Science* **1991**, *252*, 1303−1305.
(47) Ulrich, A. S.; Watts, A.; Wallat, I.; Heyn, M. P. *Biochemistry* **1994**, *33*, 5370−5375.
(48) Opella, S. J. *Nat. Struct Biol.* **1997**, *4*, 845−848.
(49) Sanders, C. R., II; Hare, B. J.; Howard, K. P.; Prestegard, J. H. *Prog. NMR Spectrosc.* **1994**, *26*, 421−444.
(50) Howard, K. P.; Opella, S. J. *J. Magn. Reson. B* **1996**, *112*, 91−94.
(51) Struppe, J.; Komives, E. A.; Taylor, S. S.; Vold, R. R. *Biochemistry* **1998**, *37*, 15523−15527.
(52) Prosser, R. S.; Hwang, J. S.; Vold, R. R. *Biophys. J.* **1998**, *74*, 2405−2418.
(53) Marassi, F. M.; Ramamoorthy, A.; Opella, S. J. *P. Natl. Aca. Sci. U.S.A.* **1997**, *94*, 8551−8556.
(54) Brenneman, M. T.; Cross, T. A. *J. Chem. Phys.* **1990**, *92*, 1483−1494.
(55) Opella, S. J.; Stewart, P. L.; Valentine, K. G. *Q. Rev. Biophys.* **1987**, *19*, 7−49.
(56) Separovic, F.; Pax, R.; Cornell, B. A. *Mol. Phys.* **1993**, *78*, 357−369.
(57) Cross, T. A.; Opella, S. J. *Curr. Opin. Struct. Biol.* **1994**, *4*, 574−581.
(58) Smith, S. O.; Peersen, O. B. *Annu. Rev. Biophys. Biomol. Struct.* **1992**, *21*, 25−47.
(59) Ketchem, R. R.; Roux, B.; Cross, T. A. *Structure* **1997**, *5*, 1655−1669.
(60) Fields, C. A.; Fields, G. B.; Noble, R. L.; Cross, T. A. *Int. J. Peptide Protein Res.* **1989**, *33*, 298−303.
(61) Smith, R.; Separovic, F.; Milne, T. J.; Whittaker, A.; Benett, F. M.; Cornell, B. A.; Makriyannis, A. *J. Mol. Biol.* **1994**, *241*, 456−466.
(62) Arkin, I. T.; Adams, P. D.; Brunger, A. T.; Smith, S. O.; Engelman, D. M. *Annu. Rev. Biophys. Biomol.* **1997**, *26*, 157−179.
(63) McDonnell, P. A.; Shon, K.; Kim, Y.; Opella, S. J. *J. Mol. Biol.* **1993**, *233*, 447−463.
(64) Tan, W. M.; Jelinek, R.; Opella, S. J.; Malik, P.; Terry, T. D.; Perham, R. N. *J. Mol. Biol.* **1999**, *286*, 787−796.
(65) Wu, C. H.; Ramamoorthy, A.; Opella, S. J. *J. Magn. Reson. A* **1994**, *109*, 270−272.
(66) Ramamoorthy, A.; Wu, C. H.; Opella, S. J. *J. Magn. Reson. B* **1995**, *107*, 88−90.

these results are encouraging and have stimulated considerable interest (including our own) in uniformly labeled oriented proteins, assignment of the signals to specific residues, either by direct $^{15}N-^{15}N$ exchange or by proton-mediated exchange,[67] remains a significant problem. In addition, the sensitivity of ^{15}N-detected experiments is inherently low due to the small magnetogyric ratio of ^{15}N nuclei, which makes signals relatively weak and $^{15}N-^{15}N$ exchange slow.

Uniformly ^{13}C- and ^{15}N-labeled proteins have several potential advantages over uniformly ^{15}N-labeled proteins as targets for structural studies by solid-state NMR. First, the sensitivity of ^{13}C NMR detection is higher than that of ^{15}N detection by a factor of approximately four (assuming identical line widths). Second, information about side chain conformations is potentially accessible, which may lead to the determination of global protein structures including side chain positions. Third, and perhaps most importantly, the use of uniform ^{13}C and ^{15}N labeling may permit sequential assignment of signals from $^{15}N/^{13}C$ and $^{13}C/^{13}C$ chemical shift correlations through polarization transfer via strong $^{15}N-^{13}C$ and $^{13}C-^{13}C$ dipolar interactions. To date, comparatively little work has been done on solid-state NMR spectroscopy of ^{15}N- and ^{13}C-labeled, oriented peptides and proteins. This is mainly because the $^{13}C-^{13}C$ dipole−dipole couplings, up to 7 kHz in magnitude, lead to significant complexity and line broadening in ^{13}C spectra of uniformly ^{15}N- and ^{13}C-labeled samples. In principle, the effects of $^{13}C-^{13}C$ couplings could be removed by nonselective homonuclear decoupling sequences, which have been developed mainly for $^{1}H-^{1}H$ decoupling in solids.[68−71] However, in the case of $^{13}C-^{13}C$ decoupling, the large distribution of chemical shifts becomes a significant hindrance. For example, in a field of 17.6 T, the chemical shift difference between CH_3 and CO amounts to 50 kHz and exceeds the useful bandwidth of existing, nonselective homonuclear decoupling sequences. Recent work by Opella and co-workers[72−74] demonstrates some of the features and advantages of combined ^{15}N- and ^{13}C-labeling, but multidimensional techniques for uniformly ^{15}N- and ^{13}C-labeled peptides and proteins with ^{13}C detection have not yet been demonstrated.

In this paper, we present a new approach to solid-state NMR studies of uniformly ^{15}N- and ^{13}C-labeled oriented peptides and proteins. Our approach depends on the detection of carbonyl and carboxyl (^{13}CO) signals with the removal of strong $^{13}C-^{13}C$ dipole−dipole couplings by a novel phase-modulated selective homonuclear (PSH) decoupling scheme. PSH decoupling permits the observation of ^{13}C-detected chemical shift spectra for CO carbons in uniformly labeled molecules. We also describe a new $^{15}N-^{13}C$ polarization transfer scheme for oriented systems in solid-state NMR, based on Hartmann−Hahn-matched WALTZ-5 irradiation. By incorporating PSH decoupling and WALTZ-5 cross-polarization into a two-dimensional (2D) chemical shift correlation measurement, we obtain good spectral resolution, sequential resonance assignment pathways, and structural constraints, all in a single ^{13}C-detected 2D spectrum. The resolution and structural information content is further increased by adding a third spectral dimension in which $^{1}H-^{15}N$ dipole−dipole couplings are recorded with a PISEMA sequence.[65,66] To our knowledge, these 2D and three-dimensional (3D) results are the first demonstration of sequential assignments in a uniformly ^{15}N- and ^{13}C-labeled oriented polypeptide. The new techniques and their implementation in one-dimensional (1D), 2D, and 3D spectroscopy are described below and demonstrated experimentally on uniformly labeled, single-crystal alanine and the tripeptide L-alanylglycylglycine (AlaGlyGly).

Materials and Methods

Solid-state NMR experiments were carried out on Bruker DMX-750 (17.6 T) and Chemagnetics Infinity-400 (9.39 T) spectrometers. Pulse sequences are described in detail below. For experiments at 17.6 T, a triple resonance probe was constructed with a 2-mm-diameter horizontal solenoid sample coil, capable of producing radio frequency (rf) fields of 120 kHz, 90 kHz, and 60 kHz with input rf powers of 25, 220, and 250 W at the ^{1}H, ^{13}C, and ^{15}N NMR frequencies, respectively. For experiments at 9.39 T, a Chemagnetics triple resonance MAS probe was fitted with a 5-mm-diameter horizontal solenoid. All measurements were performed at room temperature.

Uniformly ^{15}N- and ^{13}C-labeled AlaGlyGly was prepared by solid-phase peptide synthesis, using FMOC-protected labeled amino acids. FMOC-protected ^{15}N- and ^{13}C-labeled glycine was obtained from Cambridge Isotopes Laboratories. FMOC-protected ^{15}N- and ^{13}C-labeled L-alanine was prepared from uniformly ^{15}N- and ^{13}C-labeled L-alanine (Isotec) following the procedure of Fields et al.[60] After cleavage of the peptide from the Wang resin with 95% trifluoroacetic acid, the labeled peptide was purified by precipitation with cold acetone, dissolved in water, and lyophilized. Labeled and unlabeled (Sigma) AlaGlyGly powders were mixed in a 1:9 ratio, dissolved in a minimal amount of water, and cocrystallized by slow evaporation over a period of 3 to 10 days. A 5.3 mg crystal (2.6 μmol uniformly labeled molecules) was used in experiments at 17.6 T. A 22 mg crystal (11 μmol uniformly labeled molecules) and a 33 mg crystal (17 μmol uniformly labeled molecules) were used in experiments at 9.39 T. Dilution of uniformly labeled AlaGlyGly in unlabeled material reduces effects of intermolecular dipole−dipole couplings among ^{13}C and ^{15}N nuclei that might otherwise interfere with the assignment of resonances in the 2D and 3D spectra described below.

Single crystals of uniformly ^{15}N- and ^{13}C-labeled L-alanine (Isotec) were prepared by slow evaporation of an aqueous solution. A 18 mg crystal was used in the experiments described below.

In experiments with selective homonuclear decoupling, ^{13}C NMR signals must be acquired during the application of a pulse train to both the ^{13}C and the ^{15}N spins, with period τ (see Figure 2). At 17.6 T, typically 10 complex signal points are digitized in each window between pulses, with 0.5 μs per point. The receiver bandwidth is set to 2 MHz. At 9.39 T, typically eight complex signal points are digitized in each window, with 1 μs per point. The receiver bandwidth is set to 1 MHz. The time-domain signals are Fourier transformed after filling the gaps between sampling windows with an appropriate number of zeroes to account for the duration of the pulses and receiver deadtime. This procedure produces a series of "sideband" spectra, separated by frequency increments of τ^{-1}. Only the "centerband" spectrum is analyzed.

Simulations of $^{15}N-^{13}C$ polarization transfer leading to Figures 10 and 11 were performed with programs written specifically for this purpose. The state of the system of N spins was represented by a $2^N \times 2^N$ density matrix in the direct product basis, with initial condition equal to the matrix representation of the x component of ^{15}N spin angular momentum. The density matrix was propagated under the appropriate time-dependent $2^N \times 2^N$ spin Hamiltonian matrix in the rotating frame, including chemical shift, dipole−dipole coupling, and rf field terms. The amplitude of polarization transfer was evaluated as the trace of

(67) Ramamoorthy, A.; Gierasch, L. M.; Opella, S. J. *J. Magn. Reson. B.* **1995**, *109*, 112−116.
(68) Waugh, J. S.; Huber, L. M.; Haeberlen, U. *Phys. Rev. Lett.* **1968**, *20*, 180.
(69) Mansfield, P.; Orchard, M. J.; Stalker, D. C.; Richards, K. H. B. *Phys. Rev. B* **1973**, *7*, 90.
(70) Rhim, W. K.; Elleman, D. D.; Vaughan, R. W. *J. Chem. Phys.* **1973**, *59*, 3740.
(71) Mehring, M. *High-resolution NMR in solids*, 2nd ed.; Springer-Verlag: New York, 1983.
(72) Schneider, D. M.; Tycko, R.; Opella, S. J. *J. Magn. Reson.* **1987**, *73*, 568−573.
(73) Gu, Z.; Opella, S. J. *J. Magn. Reson.* **1999**, *138*, 193−198.
(74) Tan, W. M.; Gu, Z.; Zeri, A. C.; Opella, S. J. *J. Biomolec. NMR* **1999**, *13*, 337−342.

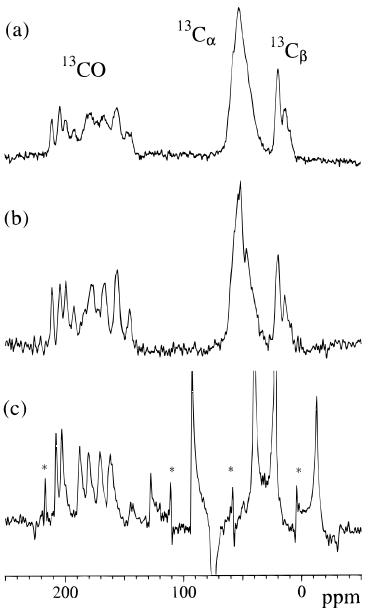

Figure 1. ^{13}C NMR spectra of a 5.3 mg single crystal of uniformly ^{15}N- and ^{13}C-labeled AlaGlyGly (10% labeled molecules diluted in 90% unlabeled molecules), observed at 188.53 MHz (17.6 T field) with ^{1}H decoupling (a), ^{1}H and ^{15}N decoupling (b), and ^{1}H and ^{15}N decoupling and phase-modulated selective homonuclear (PSH) ^{13}C decoupling (c). Contact time for ^{1}H/^{13}C cross-polarization was 0.8 ms. The amplitudes of the rf fields for cross-polarization and ^{1}H decoupling were 70.0 kHz. For c, the pulse sequence shown in Figure 2 was used. A ^{15}N decoupling pulse of $\tau_N = 4.5$ μs and a ^{13}C decoupling pulse of $\tau_C = 2.5$ μs are applied to every cycle of $\tau = 12.5$ μs. The selective ^{13}C decoupling fields were applied at the position of 57.5 ppm to decouple C_α and C_β carbons from carbonyl or carboxyl carbons. The amplitude of the rf pulses for the ^{15}N decoupling was 60 kHz, and that for the ^{13}C decoupling was 50 kHz. Hence, the average fields for ^{15}N decoupling and selective ^{13}C decoupling were 22 and 10 kHz so that they cover the spectral widths of amino and amide ^{15}N (0−250 ppm) and of $^{13}C_\alpha$ (30−80 ppm) and $^{13}C_\beta$ (0−80 ppm), respectively. The phase of ^{13}C-selective decoupling pulses was modulated as $\phi_C = 30°, 30°, 30°, 30°, -30°, -30°, -30°, -30°$ to increase the decoupling bandwidth. The phase of ^{15}N decoupling pulses was modulated as $\phi_N = 30°, 30°, -30°, -30°$. 128 FIDs were accumulated for part a, and 512 FIDs were accumulated for parts b and c.

the product of the density matrix with the x component of ^{13}C spin angular momentum for the appropriate ^{13}C nucleus.

Results

One-Dimensional ^{13}C NMR Spectroscopy. Figure 1 shows 1D ^{13}C spectra of the 5.3 mg uniformly ^{15}N- and ^{13}C-labeled AlaGlyGly crystal in an arbitrary orientation (determined below), obtained at 17.6 T (749.6 MHz ^{1}H NMR frequency; 188.5 MHz ^{13}C NMR frequency), with proton decoupling (Figure 1a), proton and ^{15}N decoupling (Figure 1b), and proton, ^{15}N, and phase-modulated selective ^{13}C decoupling (Figure 1c). These spectra amply illustrate the inherent complexity of ^{13}C spectra of uniformly labeled, oriented molecules. ^{13}C magnetization is prepared by cross-polarization (CP) from protons[75,76] in all cases. Signals from ^{13}CO, $^{13}C_\alpha$, and $^{13}C_\beta$ spins can be distinguished in Figure 1a, but signals within each group cannot be resolved because of significant broadening due to the ^{13}C−^{13}C and ^{13}C−^{15}N dipole−dipole couplings. The ^{13}CO region (150−210 ppm) exhibits sharper lines in Figure 1b, but these lines are still split

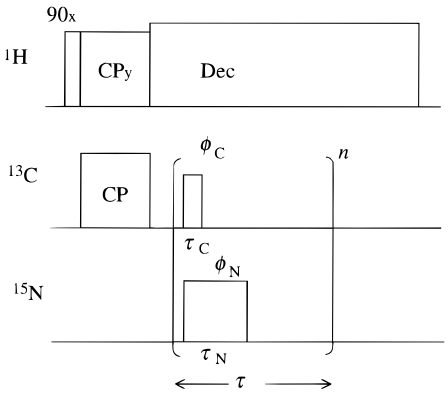

Figure 2. Pulse sequence for observing ^{13}C NMR spectra under ^{15}N decoupling and ^{13}C selective homonuclear decoupling. After ^{13}C magnetization was prepared by cross polarization, signals were sampled during intervals between ^{15}N and selective ^{13}C decoupling pulses. Phases of the decoupling pulses ϕ_C and ϕ_N are modulated, if indicated. τ_C and τ_N denote pulse widths for ^{13}C decoupling and ^{15}N decoupling pulses, respectively. τ denotes the repetition time for decoupling pulses.

and broadened by ^{13}C−^{13}C dipolar couplings. ^{13}C−^{13}C dipolar couplings must be removed to make spectral analysis possible and to extract structural information from the spectra. To overcome this problem, the PSH decoupling sequence shown in Figure 2 was developed to decouple C_α and aliphatic side chain carbons from carbonyl and carboxyl carbons. Following cross-polarization, a train of pulses of length τ_C is applied at a carrier frequency in the aliphatic region of the ^{13}C spectrum (57.5 ppm in Figure 1). The individual pulses are separated by delays of length $\tau - \tau_C$ during which the ^{13}C NMR signals are digitized. The phases of these selective decoupling pulses follow the pattern $+\phi_C, +\phi_C, +\phi_C, +\phi_C, -\phi_C, -\phi_C, -\phi_C, -\phi_C$. A similar pulse train is also applied to ^{15}N spins for ^{15}N decoupling, with pulse lengths τ_N and phases $\pm\phi_N$, but this train works as broadband heteronuclear TPPM decoupling.[77] The ^{15}N rf carrier frequency is set to the middle of the amide nitrogen region. Short pulses are used for ^{15}N decoupling, rather than continuous irradiation, to avoid excess noise in the ^{13}C signal acquisition windows. Six lines are clearly observed in the ^{13}CO region of Figure 1c, corresponding to the two carbonyl carbons and one carboxyl carbon of each of the two magnetically inequivalent AlaGlyGly molecules in the unit cell of the crystal structure.[78,79] These lines are separated and resolved due to the large carbonyl and carboxyl CSAs, which span approximately 150 ppm. Thus, PSH decoupling permits the observation of a well-resolved ^{13}CO chemical shift spectrum in a uniformly labeled, oriented system.

The ^{13}CO line widths in Figure 1c range from 2.0 to 3.5 ppm, with lines closer to the PSH carrier frequency exhibiting the larger widths. The line broadening is attributed to rf inhomogeneity, as discussed below.

In addition to the ^{13}CO lines, large peaks from −30 to 100 ppm and smaller peaks around 120 ppm are apparent in Figure 1c. These peaks are caused by nutation of $^{13}C_\alpha$ and $^{13}C_\beta$ magnetization about the effective rf field of the selective decoupling pulses and could therefore be suppressed by presaturation of the $^{13}C_\alpha$ and $^{13}C_\beta$ magnetization. In the 2D and 3D heteronuclear correlation experiments described below, these peaks are suppressed by the polarization transfer pathway. In

(75) Hartmann, S. R.; Hahn, E. L. *Phys. Rev.* **1962**, *128*, 2042.
(76) Pines, A.; Gibby, M. G.; Waugh, J. S. *J. Chem. Phys.* **1973**, *59*, 569.
(77) Bennett, A. E.; Rienstra, C. M.; Auger, M.; Lakshmi, K. V.; Griffin, R. G. *J. Chem. Phys.* **1995**, *103*, 6951−6958.
(78) Subramanian, E.; Lalitha, V. *Biopolymers* **1983**, *22*, 833−838.
(79) Lalitha, V.; Subramanian, E.; Bordner, J. *Ind. J. Pure Appl. Phys.* **1985**, *23*, 506−508.

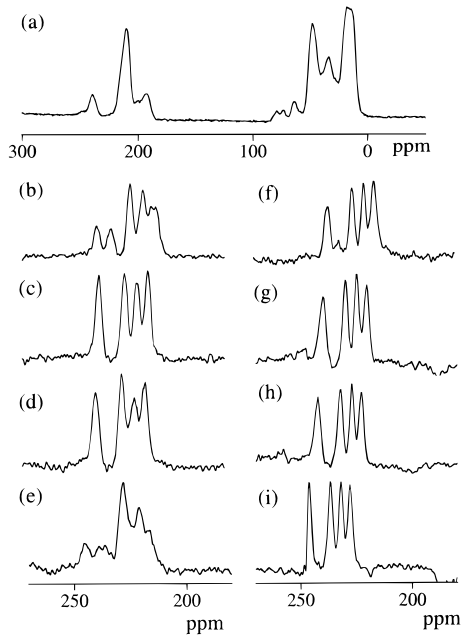

Figure 3. ^{13}C NMR spectra of an 18 mg single crystal of uniformly ^{15}N- and ^{13}C-labeled L-alanine, observed at 100.8 MHz (9.39 T field), with ^{1}H and ^{15}N decoupling (a), with ^{1}H and ^{15}N decoupling and selective homonuclear ^{13}C decoupling (b−e), and with ^{1}H and ^{15}N decoupling and phase-modulated selective homonuclear ^{13}C decoupling (f−i). Carrier frequency for selective ^{13}C decoupling was set at (b, f) 3 ppm, (c, g) 23 ppm, (d, h) 33 ppm, and (e, i) 53 ppm. The pulse sequence shown in Figure 2 was used for (b−i). $\tau_C = 3.6$ μs, $\tau_N = 12$ μs, $\tau = 17$ μs. $\phi_N = 0$. The amplitude of the rf pulses for ^{15}N decoupling was 20 kHz, and that for ^{13}C decoupling was 45 kHz. For (b−e) and (f−i), $\phi_c = 0°$ and $\phi_c = 30°$, 30°, 30°, −30°, −30°, −30°, respectively.

any event, these peaks lie outside of the ^{13}CO region of the spectrum and hence do not interfere with the analysis of the 1D, 2D, or 3D spectra. The sharp peaks in Figure 1c near 6, 57, 111, and 219 ppm are cycling sidebands[80,81] caused by the phase modulation of the decoupling pulses.

The increased decoupling bandwidth of PSH decoupling, compared with unmodulated selective decoupling, is illustrated in Figure 3, which shows ^{13}C NMR spectra of a single crystal of uniformly ^{15}N- and ^{13}C-labeled L-alanine. The spectrum in Figure 3a, obtained with ^{1}H and ^{15}N decoupling only, exhibits broadening due to ^{13}C-$^{-3}$C dipolar couplings. Figure 3b−e show the dependence of the carboxyl region of the spectrum on the rf carrier frequency used for selective decoupling, without phase modulation. With the carrier frequency at 23 or 33 ppm (Figure 3c,d), four carboxyl lines from the four magnetically inequivalent molecules in the unit cell[82] are obtained. With the carrier frequency at 3 or 53 ppm (Figure 3b,e), these lines are significantly broadened and split by residual homonuclear couplings. Figure 3f−i show the corresponding spectra with phase-modulated selective decoupling. Four sharp carboxyl lines are observed over the entire 50 ppm range of rf carrier frequencies.

Selective decoupling of aliphatic carbons causes shifts of the apparent ^{13}CO resonance positions because, during the signal detection period, the ^{13}C spins precess about an effective magnetic field whose magnitude is determined by the resonance offsets ω_S, the average rf field ω_{av}, and the phase modulation (see the Appendix for theoretical details). These shifts are somewhat analogous to the well-known chemical shift scaling in nonselective homonuclear decoupling techniques (e.g., WAHUHA or Lee−Goldburg decoupling) but are nonlinear functions of the resonance offsets, decreasing with increasing ω_{av}/ω_S and therefore becoming less significant at higher static fields. The shifts are independent of the homonuclear couplings, as has been verified by numerical simulations of the effects of selective decoupling on a coupled three-spin system with realistic parameters for the ^{13}CO, $^{13}C_\alpha$, and $^{13}C_\beta$ carbons of an amino acid residue in a polypeptide (data not shown). Hence, the shifts can be easily simulated without knowledge of the structural parameters. The shifts can also be calibrated experimentally using standard liquid samples or selectively labeled crystals with isolated ^{13}C nuclei, as is commonly done in nonselective homonuclear decoupling experiments. Figure 4 shows a calibration curve for the shifts in apparent resonance positions, experimentally obtained using a 1-^{13}C glycine crystal at several orientations. With such a calibration curve, the observed ^{13}CO resonance positions are readily converted to the true chemical shifts, which in turn provide structural information.

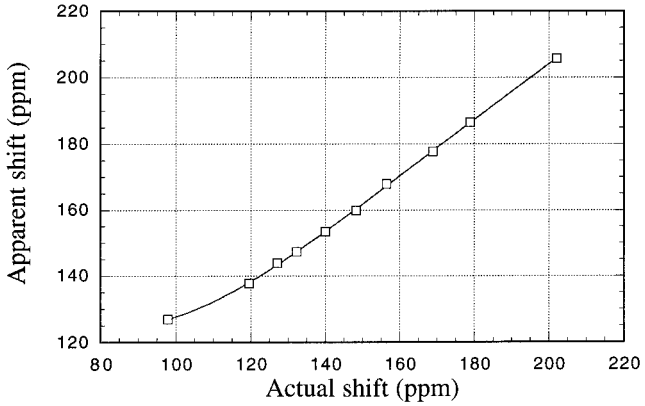

Figure 4. Calibration curve for ^{13}C NMR frequency shifts due to the PSH decoupling field. Actual chemical shifts were observed for a single crystal of 1-^{13}C glycine at a series of arbitrary orientations. Apparent shifts were obtained for the same sample under the PSH decoupling sequence shown in Figure 2. Experimental parameters were the same as those used for Figure 1.

One-Dimensional ^{15}N NMR Spectroscopy. Figure 5 shows ^{15}N spectra of the 5.3 mg uniformly ^{15}N- and ^{13}C-labeled AlaGlyGly crystal in the same orientation as in Figure 1. With proton decoupling alone (Figure 5a), the spectrum is very complex due to ^{13}C−^{15}N dipole−dipole couplings. With proton and cw ^{13}C decoupling (Figure 5b), the spectrum is somewhat simplified but the ^{15}N NMR lines are still broadened by residual ^{13}C−^{15}N couplings. This is because the ^{13}C chemical shift range of peptides is approximately 55 kHz in the 17.6 T field and the decoupling field amplitude is 25 kHz. Hence, resonance offset effects are significant. Higher rf power for ^{13}C decoupling would produce narrower ^{15}N lines but, as in most NMR techniques for studies of biopolymers, it is advisable to avoid high rf powers in order to minimize sample heating. The use of phase-modulated, broadband decoupling sequences developed for liquid-state NMR[81] is an alternative solution. Figure 5c shows the ^{15}N NMR spectrum obtained with WALTZ-16[80,83] ^{13}C decoupling. The resolution is enhanced by a factor of 5. We

(80) Shaka, A. J.; Keeler, J. M.; Freeman, R. *J. Magn. Reson.* **1983**, *53*, 313−340.

(81) Ernst, R. R.; Bodenhousen, G.; Wokaun, A. *Principles of Nuclear Magnetic Resonance in One and Two Dimensions*, 1st ed.; Oxford University Press: Oxford, 1987.

(82) Naito, A.; Ganapathy, S.; Akasaka, A.; McDowell, C. A. *J. Chem. Phys.* **1981**, *74*, 3190−3197.

(83) Shaka, A. J.; Keeler, J.; Frenkiel, T.; Freeman, J. *J. Magn. Reson.* **1983**, *52*, 335−338.

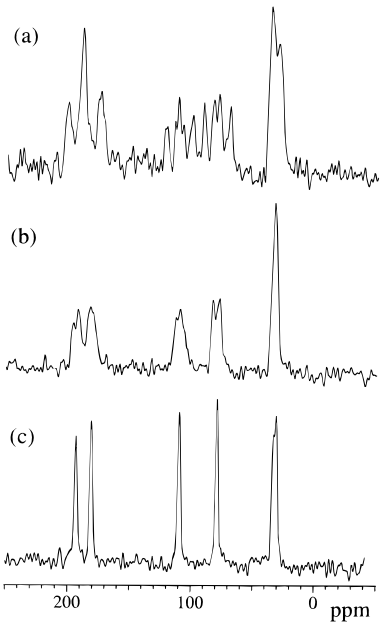

Figure 5. ^{15}N NMR spectra of a 5.3 mg crystal of uniformly ^{15}N- and ^{13}C-labeled AlaGlyGly (10% labeled molecules diluted in 90% unlabeled molecules) observed at 75.98 MHz (17.6 T field) with (a) ^{1}H TPPM decoupling, (b) ^{1}H TPPM decoupling and ^{13}C cw decoupling, and (c) ^{1}H TPPM decoupling and ^{13}C WALTZ-16 decoupling. The orientation of the crystal was the same as in Figure 1. The rf amplitudes were 55.5, 85, and 25 kHz for cross polarization, ^{1}H decoupling, and ^{13}C decoupling, respectively. A total of 512 scans were accumulated for all the spectra.

also confirmed that TPPM ^{13}C decoupling works as a broadband decoupling sequence but, in a field of 17.6 T, the ^{15}N resolution with WALTZ-16 is superior by a factor of 1.5. Considering the distributions of the CSA in amide ^{15}N (50−220 ppm)[84,85] and amino ^{15}N, the two overlapping lines near 30 ppm in Figure 5c may be assigned to amino ^{15}N. The other four lines are assigned to the amide ^{15}N of the two magnetically inequivalent AlaGlyGly molecules in the crystal. The amide ^{15}N line widths in Figure 5c are 2.5 ppm.

Two-Dimensional Heteronuclear Shift Correlation Spectroscopy. Figure 6a shows a 2D ^{15}N/^{13}C chemical shift correlation spectrum of the 22 mg uniformly ^{15}N- and ^{13}C-labeled AlaGlyGly crystal at an arbitrary orientation (determined below), obtained at 9.39 T (100.8 MHz ^{13}C and 40.6 MHz ^{15}N frequencies). Figure 6b shows representative 1D slices. The pulse sequence used for this ^{13}C-detected experiment is shown in Figure 7. Six ^{13}C and six ^{15}N resonances are expected in Figure 6, because of the two magnetically inequivalent AlaGlyGly molecules. All of these resonances are in fact observed and can be sequentially assigned, as summarized in Table 1. Sequential assignments are possible because the ^{15}N resonances exhibit cross-peaks both to directly bonded ^{13}CO carbons (e.g., ^{15}N of Gly2 to ^{13}CO of Ala1) and to ^{13}CO carbons that are two bonds away (e.g., ^{15}N of Gly2 to ^{13}CO of Gly2). In addition, weak cross-peaks from ^{15}N of Gly3 to ^{13}CO of Ala1, separated by four bonds, are observed. Although the cross-peaks between directly bonded ^{15}N and ^{13}CO generally have the highest intensity, this is not always true because of variations in ^{15}N/^{13}C and ^{1}H/^{15}N polarization transfer efficiencies primarily due to the orientation dependences of the dipole−dipole couplings

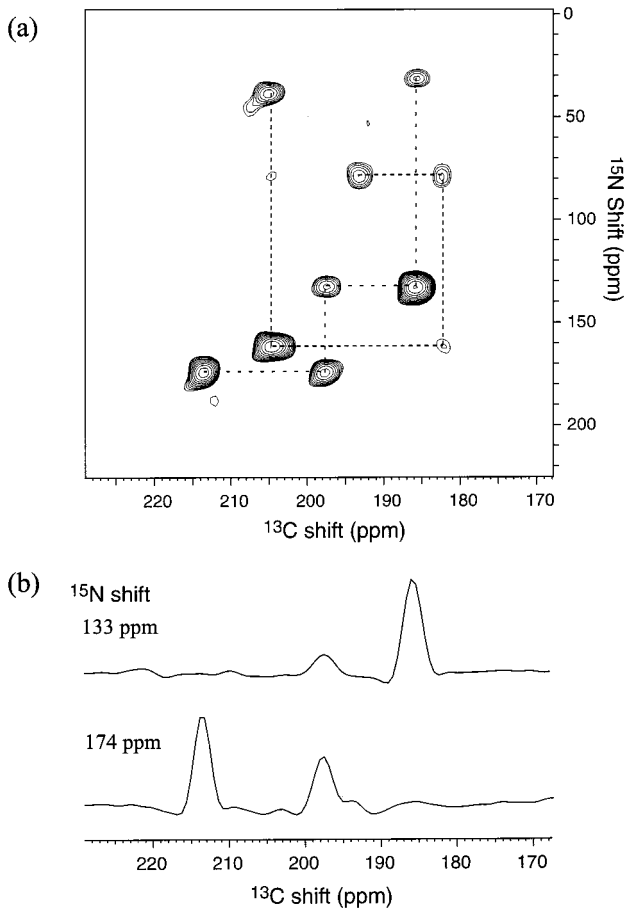

Figure 6. (a) Two-dimensional ^{15}N/^{13}C chemical shift correlation spectrum for a 22 mg single crystal of uniformly ^{15}N- and ^{13}C-labeled AlaGlyGly (10% labeled molecules diluted in 90% unlabeled molecules), observed at 100.8 MHz (9.39 T), using the pulse sequence shown in Figure 7 with $\tau_m = 2.5$ ms. The amplitude for ^{1}H decoupling was 95 kHz. During the t_1 period, ^{13}C TPPM decoupling with an rf amplitude of 27 kHz was applied. The ^{15}N and ^{13}C rf amplitudes during the WALTZ-5 cross-polarization period were 27 kHz, and rf carrier frequencies were set to 90 and 160 ppm for ^{15}N and ^{13}C, respectively. The flip angle α in the WALTZ-5 sequence was 90°. During the t_2 period, the rf amplitudes were 55 kHz and 27 kHz for ^{13}C PSH decoupling and ^{15}N pulsed TPPM decoupling, respectively. $\tau_C = 4.5$ μs, $\tau_N = 13$ μs, and $\tau = 26$ μs. Carrier frequency for ^{13}C PSH decoupling was set at 37.8 ppm. 84 complex t_1 points were acquired, with a t_1 increment of 40 μs and 300 scans for the real and imaginary components of each point. (b) One-dimensional slices of the two-dimensional spectrum, at the indicated ^{15}N chemical shifts.

(see below). Based on ^{15}N chemical shifts, the ^{15}N resonances at 31.5 and 38.6 ppm can be assigned to amino nitrogens of Ala1. This assignment can also be made by observing that each of these resonances has only one cross-peak with ^{13}CO because of the absence of a directly bonded carbonyl carbon. Similarly, the ^{13}CO resonances at 193.0 and 213.4 ppm have only one cross-peak, so they may be assigned to carboxyl carbons of Gly3 because of the absence of directly bonded nitrogens.

The pulse sequence for ^{13}C-detected 2D shift correlation (Figure 7) uses standard cross-polarization to prepare transverse ^{15}N magnetization. This magnetization precesses at the ^{15}N chemical shift frequencies during t_1 under high-power TPPM proton decoupling[77] and ^{13}C decoupling. Either the x or the y component of ^{15}N magnetization is stored as longitudinal magnetization by a $\pi/2$ pulse at the end of t_1. After a dephasing delay (1 ms), the magnetization is transferred to ^{13}C nuclei by

(84) Shoji, A.; Ozaki, T.; Fujito, T.; Deguchi, K.; Ando, S.; Ando, I. *Macromolecules* **1989**, *22*, 2860−2863.

(85) Duncan, T. M. *A compilation of chemical shift anisotropies*; The Farragut Press: Chicago, 1990.

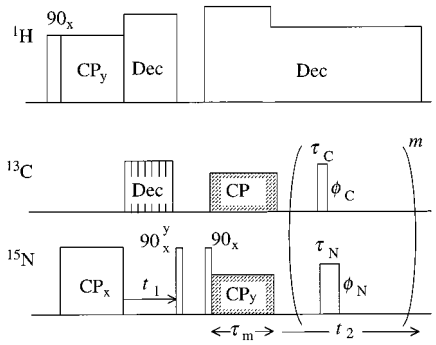

Figure 7. Pulse sequence for 2D ^{15}N/^{13}C chemical shift correlation spectroscopy for uniformly ^{15}N- and ^{13}C-labeled oriented peptides. In the t_1 period, ^{15}N magnetization prepared by ^{1}H/^{15}N cross-polarization evolves under ^{1}H decoupling and WALTZ-16 or TPPM ^{13}C decoupling. ^{15}N/^{13}C polarization transfer is accomplished by application of Hartmann−Hahn-matched WALTZ-5 sequences to ^{15}N and ^{13}C nuclei. In the t_2 period, ^{13}C signals in the carbonyl and carboxyl region are detected under PSH ^{13}C decoupling and ^{15}N decoupling. See the text for further details.

Table 1. Summary of Chemical Shift Assignments from Two-Dimensional Heteronuclear Shift Correlation Spectrum in Figure 6

		^{15}N chemical shift (ppm)		^{13}CO chemical shift (ppm)	
		exptl	simulated[c]	exptl (calibrated)[b]	simulated[c]
AlaGlyGly	Ala1	31.5	NA	185.5 (121.0)	186.9
Molecule A[a]	Gly2	133.0	108.9	197.6 (159.1)	199.8
	Gly3	174.3	186.5	213.4 (188.0)	213.2
AlaGlyGly	Ala1	38.6	NA	205.1 (173.7)	207.9
Molecule B[a]	Gly2	161.3	134.2	183.3 (102.0)	184.0
	Gly3	78.5	97.5	193.0 (148.3)	191.4

[a] Molecules A and B refer to the two magnetically inequivalent AlaGlyGly molecules in the crystal unit cell. [b] Experimental chemical shifts refer to apparent ^{13}C shifts shown in Figure 6, which contain extra shifts due to the selective decoupling fields. Calibrated shifts denote actual ^{13}C shifts after the extra shifts are subtracted. [c] Magnetic field direction was chosen to minimize the RMSD between experimental and simulated ^{13}CO shifts only. Simulated shifts were calculated based on the known crystal structure[78,79] and principal axis values[20] and the tensor orientations from model peptides.[20,82,89]

a ^{15}N/^{13}C cross-polarization period of duration τ_m (2.5 ms in Figure 7). During the polarization transfer period, WALTZ-5 sequences (*RRRR*α, with $R = 90_y180_{-y}270_y$ and $\alpha = \alpha_y$), which consist of WALTZ-4[83] sequences and short spin lock pulses with a flip angle of α, are applied synchronously to both the ^{15}N and the ^{13}C spins, with Hartmann−Hahn-matched rf field amplitudes. Use of WALTZ-5 sequences for cross-polarization (WALTZ-5 CP) increases the range of ^{15}N and ^{13}C frequencies over which Hartmann−Hahn matching can be achieved. Cw proton decoupling is applied during ^{15}N/^{13}C WALTZ-5 CP. ^{13}C NMR signals are detected during t_2, with PSH ^{13}C decoupling, phase-modulated pulsed ^{15}N decoupling, and cw proton decoupling, as in Figure 2.

Experimental polarization transfer efficiencies using WALTZ-5 CP, defined as the ratio of ^{13}CO signal intensities following sequential ^{1}H/^{15}N cross-polarization and ^{15}N/^{13}C WALTZ-5 CP to signal intensities following ^{1}H/^{13}C cross-polarization alone, were found to be approximately 0.40 with $\tau_m = 1$ ms and 0.25 for $\tau_m = 2$ ms for AlaGlyGly at both 17.6 and 9.39 T. Assuming ideal ^{1}H/^{13}C and ^{1}H/^{15}N cross-polarization and complete equilibration of ^{15}N and ^{13}C spin polarizations during polarization transfer, the theoretical maximum efficiency would be 0.5. Other approaches to ^{15}N/^{13}C polarization transfer were tested, including cw Hartmann−Hahn cross-polarization, ramped-amplitude cross-polarization, and ramped-frequency cross-polarization. These approaches gave similar polarization transfer efficiencies for single ^{13}CO lines, but were not capable of uniform polarization transfer across the ^{13}CO spectral range. The spurious peaks due to nutation of $^{13}C_\alpha$ and $^{13}C_\beta$ magnetization that appear in the 1D ^{13}C spectra with PSH decoupling (Figure 1c) are strongly attenuated in the 2D spectrum. This is because the WALTZ-5 CP sequence transfers polarization from ^{15}N nuclei primarily to ^{13}CO, rather than $^{13}C_\alpha$ and $^{13}C_\beta$ nuclei.

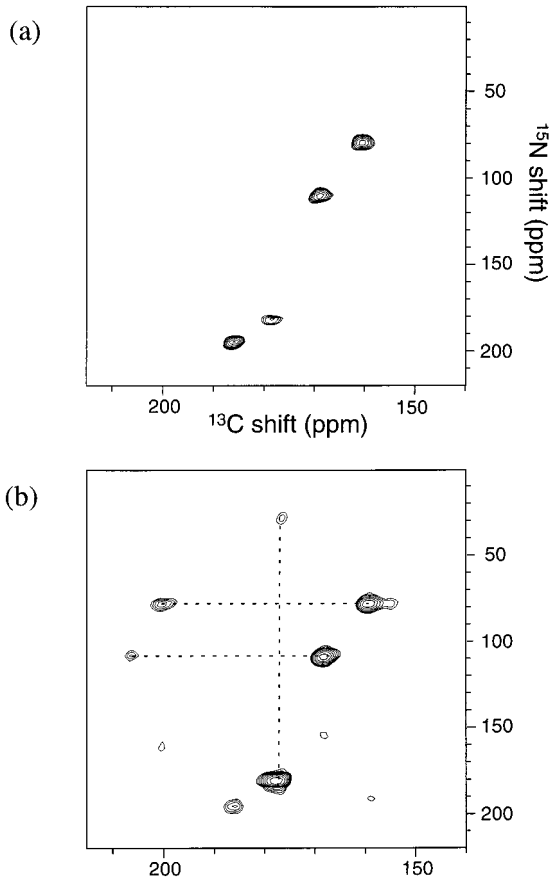

Figure 8. ^{15}N/^{13}C correlation spectrum for a 5.3 mg crystal of uniformly ^{15}N- and ^{13}C-labeled AlaGlyGly (10% labeled molecules diluted in 90% unlabeled molecules), observed at 188.53 MHz (17.6 T field) with $\tau_m = 1.3$ ms (a) and $\tau_m = 2.6$ ms (b). Pulse sequence shown in Figure 7 was used. During the t_1 period, WALTZ-16 ^{13}C decoupling and ^{1}H TPPM decoupling were applied with rf amplitudes of 25 and 90 kHz, respectively. During the polarization transfer period, rf amplitudes were 25 and 100 kHz for WALTZ-5 CP and ^{1}H cw decoupling, respectively. The flip angle α in the WALTZ-5 sequence was 90°. The rf amplitudes during the t_2 period were 50, 55, and 70 kHz for PSH ^{13}C decoupling, ^{15}N decoupling, and ^{1}H decoupling, respectively. Carrier frequency of ^{13}C selective decoupling was set at 57.5 ppm. $\tau_C = 2.5$ μs, $\tau_N = 4.5$ μs, and $\tau = 12.5$ μs. 55 complex t_1 points were acquired, with a t_1 increment of 46 μs. 144 scans for the real and imaginary components of each point were used in part a and 344 scans in part b.

Figure 8 shows 2D ^{15}N/^{13}C shift correlation spectra of the 5.3 mg uniformly ^{15}N- and ^{13}C-labeled AlaGlyGly crystal used for the data in Figures 1 and 5, at the same orientation, obtained at 17.6 T (188.5 MHz ^{13}C and 76.0 MHz ^{15}N frequencies). Figure 8a shows only four cross-peaks because of the short contact time ($\tau_m = 1.3$ ms) used for WALTZ-5 CP. These cross-peaks are attributed to the directly bonded amide ^{15}N and

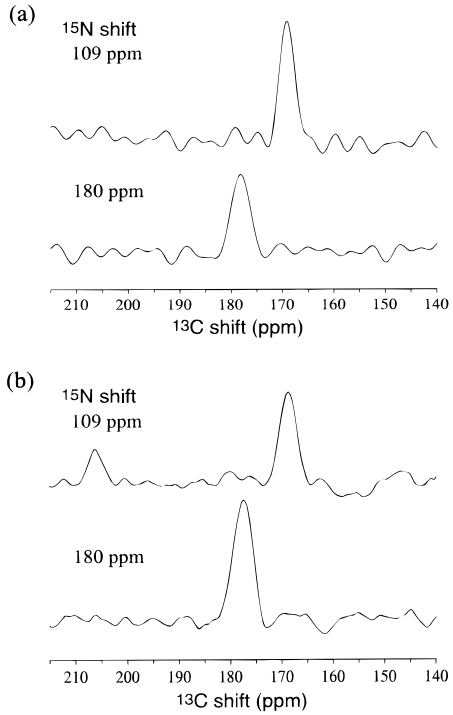

Figure 9. (a) One-dimensional slices of the two-dimensional spectrum in Figure 8a. (b) One-dimensional slices of the two-dimensional spectrum in Figure 8b. Slices are taken at the indicated ^{15}N chemical shifts.

carbonyl ^{13}C pairs of the two magnetically inequivalent molecules. Three additional cross-peaks, attributable to ^{15}N/^{13}CO pairs separated by two bonds, are observed in Figure 8b with a longer contact time ($\tau_m = 2.6$ ms). In contrast to Figure 6, the cross-peaks for nondirectly bonded pairs are weak and are not all observable. Figure 9 shows representative slices of the 2D spectra in Figure 8. Because two-bond cross-peaks linking the amide ^{15}N and ^{13}CO of Gly2 are missing in Figure 8b, full sequential assignments cannot be made. Nonetheless, with the assumption that the cross-peaks in Figure 8a arise only from directly bonded pairs, partial assignments can be made (to residue number, but not to inequivalent molecule), as summarized in Table 2. This assumption is confirmed by the calculations described below.

The ^{13}CO and ^{15}N line widths are 2−3 and 10 ppm, respectively, in Figure 6. The ^{13}CO and ^{15}N line widths are 3−5 and 6 ppm, respectively, in Figure 8. The ^{15}N line widths in the 2D spectra are limited simply by the number of t_1 points acquired, as can be seen by comparison with Figure 5c. The ^{13}CO line widths are limited by rf inhomogeneity due to the large sample size relative to the rf coil in the NMR probe (e.g., a 5 mm long, 1.5 mm diameter crystal in a 5 mm long, 2.0 mm inner diameter coil in experiments at 17.6 T). Rf inhomogeneity results in small variations in the PSH decoupling-induced frequency shifts and consequent inhomogeneous line broadening. Thus, for experiments on larger peptides or proteins, the resolution in the 2D spectra could be increased significantly by acquiring additional t_1 points and improving the homogeneity of the rf fields.

The absence of some of the expected two-bond cross-peaks in Figure 8b is due to the fact that even the WALTZ-5 CP sequence, with rf field amplitudes of 25 kHz, does not cover sufficient spectral widths at 17.6 T to permit all two-bond ^{15}N/^{13}C polarization transfers, although the one-bond polarization transfers are readily observed. This is because the two-bond

Table 2. Summary of Chemical Shift Assignments from Two-Dimensional Heteronuclear Shift Correlation Spectra in Figure 8

		^{15}N chemical shift (ppm)		^{13}CO chemical shift (ppm)	
		exptl	simulated[c]	exptl (calibrated)[b]	simulated[c]
AlaGlyGly	Ala1	missing	NA	187.2 (179.9)	187.7
Molecule A[a]	Gly2	194.5	186.5	159.2 (147.0)	154.7
	Gly3	77.4	114.7	201.9 (197.4)	204.3
AlaGlyGly	Ala1	28.7	NA	178.8 (169.9)	180.6
Molecule B[a]	Gly2	180.4	175.5	168.6 (158.0)	164.1
	Gly3	108.8	142.1	207.8 (204.5)	212.5

[a] Molecules A and B refer to the two magnetically inequivalent AlaGlyGly molecules in the crystal unit cell. As discussed in the text, assignments to inequivalent molecules are based in part on the comparison of experimental and simulated shifts. [b] Experimental chemical shifts refer to apparent ^{13}C shifts shown in Figure 6, which contain extra shifts due to the selective decoupling fields. Calibrated shifts denote actual ^{13}C shifts after the extra shifts are subtracted. [c] Magnetic field direction was chosen to minimize the RMSD between experimental and simulated ^{13}CO shifts only. Simulated shifts were calculated based on the known crystal structure[78,79] and principal axis values[20] and the tensor orientations from model peptides.[20,82,89]

polarization transfers are largely mediated by intervening $^{13}C_\alpha$ nuclei, and the total ^{13}C chemical shift range is approximately 35 kHz at 17.6 T, compared with 19 kHz at 9.39 T. Numerical simulations of polarization transfer in a heteronuclear three-spin system, representing the carbonyl carbon, the alpha carbon and the amide nitrogen of an amino acid residue in a polypeptide, support this explanation for the difference between the results in Figures 6 and 8. In these simulations, we calculate the carbonyl ^{13}C NMR signal amplitude following the application of Hartmann−Hahn-matched WALTZ-5 sequences to ^{13}C and ^{15}N spins, with initial magnetization on ^{15}N only. Only dipole−dipole couplings between directly bonded nuclei are included. Figure 10 shows the dependence of the carbonyl ^{13}C NMR signal on the polarization transfer time, for various resonance offsets of the α carbon. At small α carbon offsets, representing low fields, the carbonyl signal exhibits rapid oscillation and a large amplitude, corresponding to rapid and efficient polarization transfer. At large α carbon offsets, representing high fields, the carbonyl signal exhibits a slow buildup and a smaller amplitude. These theoretical results indicate that two-bond polarization transfer from amide ^{15}N to ^{13}CO is sensitive to the resonance offset of the intervening $^{13}C_\alpha$, in agreement with the experimental observation of decreased two-bond polarization transfer efficiency at 17.6 T.

In peptides and proteins with hydrogen-bonded secondary structure, the possibility of nonsequential ^{15}N/^{13}CO cross-peaks due to polarization transfer across hydrogen bonds may be considered. Such cross-peaks are expected to be considerably weaker than the two-bond cross-peaks discussed above, because the longer ^{15}N−^{13}C distances across hydrogen bonds imply maximum ^{15}N−^{13}C dipole−dipole couplings that are roughly four times weaker than the maximum two-bond coupling. Direct ^{15}N/^{13}C polarization transfer rates are proportional to the square of the coupling. In addition, the lack of an intervening $^{13}C_\alpha$ in the hydrogen-bonded case eliminates the possibility of indirect polarization transfer through one-bond couplings, which plays an important role in the two-bond polarization transfer along the peptide backbone (see below). Cross-peaks due to polarization transfer across hydrogen bonds are therefore not expected to interfere with sequential assignments.

Comparison of Experimental Two-Dimensional Spectra with AlaGlyGly Crystal Structure. To confirm the validity

of the above resonance assignments, we simulated the resonance positions for ^{13}CO and amide ^{15}N chemical shifts based on the known crystal structure[78,79] and suitable CSA tensor principal values and orientations. In these simulations, the orientation of the carbonyl ^{13}CO CSA tensors was fixed at the orientation used in the analysis of earlier solid-state NMR measurements on polycrystalline AlaGlyGly,[13,20,86] namely with the σ_{11} and σ_{22} axes in the plane of the peptide bond and with an angle of 130° between with σ_{22} axis and the N−CO bond. This orientation is based on studies of model dipeptides[87] and is supported by the success of the analysis of the earlier AlaGlyGly measurements.[13,20,86] The orientation of amide ^{15}N CSA tensors can have larger variations, up to 45°.[88] In these simulations, we assumed that the σ_{11} and σ_{33} axes of the ^{15}N CSA tensor are in the peptide plane and the σ_{11} axis tilts from the N−H bond to the N−CO bond by 20°.[88,89] The ^{15}N CSA principal values (σ_{11}, σ_{22}, σ_{33}) of Gly-2 and Gly-3 were determined to be (207 ± 2, 58 ± 5, 49 ± 5) and (226 ± 2, 68 ± 3, 33 ± 3) ppm by analyzing MAS sideband patterns[90] of $^{15}N_3$-AlaGlyGly obtained at a spinning frequency of 520 Hz. ^{15}N signal assignments were obtained by comparing the MAS spectrum of $^{15}N_3$-AlaGlyGly with that of $^{15}N_2$-AlaGlyGly labeled at the Ala1 and Gly2 sites. ^{13}C CSA principal values for carbonyl carbons in AlaGlyGly were taken from Weliky et al.[20] The CSA principal values of the Gly3 carboxyl carbons were determined to be (σ_{11}, σ_{22}, σ_{33}) = (249 ± 2, 188 ± 2, 100 ± 2) ppm by MAS sideband analysis. The σ_{33} axes of carboxyl CSA tensors were taken to be perpendicular to the carboxyl plane. The σ_{11} axes were assumed to bisect the C−O bonds.[82]

Chemical shifts of ^{13}CO and amide ^{15}N were calculated for various directions of the static magnetic field relative to the monoclinic crystal unit cell, as defined by azimuthal and polar angles α and β in a Cartesian coordinate system with x and y axes along the **a** and **b** lattice vectors and z axis along $\mathbf{c}' = \mathbf{a} \times \mathbf{b}$. The field direction was optimized in 5° increments in both angles to minimize the root-mean-squared deviation (RMSD) of simulated chemical shifts from experimental chemical shifts, because the field direction relative to the crystal unit cell was unknown in our experiments. Because of the ambiguity of the amide ^{15}N CSA tensor orientation, the optimization of the field direction was done to minimize the RMSD for only ^{13}CO chemical shifts. Tables 1 and 2 show simulated and experimental ^{13}CO and amide ^{15}N chemical shifts for the optimized crystal orientation, for experimental data in Figures 6 and 8. Simulated ^{13}CO shifts are in excellent agreement with experimental shifts, considering that only two adjustable parameters (i.e., α and β) were used to fit six experimental shifts. The optimal (α,β) values were (120°,160°) for Table 1 and (160°,15°) for Table 2. Although simulated ^{15}N shifts differ from experimental shifts by up to 27 ppm in Tables 1 and 37 ppm in Table 2, these differences can be attributed to deviation of the true ^{15}N CSA tensor orientation from the standard orientation adopted in the simulations. Changes in the ^{15}N CSA tensor orientation by 20° can cause changes in the shifts up to 30 ppm.

The good agreement between simulated and experimental shifts in Table 1, particularly the ^{13}CO shifts, supports the validity of the sequential resonance assignments that were derived entirely from the experimental spectrum in Figure 6.

Table 3. Cross-Peak Volumes (Arbitrary Units) in Two-Dimensional ^{15}N/^{13}C Chemical Shift Correlation Spectrum of Uniformly ^{15}N- and ^{13}C-Labeled AlaGlyGly at 9.39 T (Figure 6)

$^{15}N_i$ site	two-bond cross-peak to $^{13}CO_i$	one-bond cross-peak to $^{13}CO_{i-1}$
Ala1, molecule A	13	
Gly2, molecule A	24	160
Gly3, molecule A	96	50
Ala1, molecule B	35	
Gly2, molecule B	4	121
Gly3, molecule B	24	12

Additional considerations supporting the validity of these assignments are as follows: (1) The labeled AlaGlyGly molecules are diluted in unlabeled material, so intermolecular polarization transfer cannot lead to erroneous assignments. (2) The ^{13}CO chemical shift assignments were made independently of the connectivities in the 2D spectrum by fitting the calculated ^{13}CO shifts while varying the field direction, as described above. The best fit was found to occur with the assignments in Table 1 and a field direction of (α,β) = (120°,160°), with an RMSD of 1.7 ppm. The lowest RMSD for alternative assignments was 5.2 ppm, which is significantly greater. (3) As a test for sensitivity to the assumed ^{13}CO CSA tensor orientations, the tensor orientations were varied by ±10° in the simulations. This did not change the assignments that gave the lowest RMSD. (4) The assumed carbonyl CSA tensor orientations for AlaGlyGly have already been shown to be consistent with 2D MAS exchange[20,86] and constant-time double-quantum-filtered dipolar recoupling[13] measurements on doubly-^{13}C-labeled, polycrystalline samples, so it is not possible that these carbonyl CSA tensor orientations are greatly in error. The CSA principal values are experimentally determined, not assumed. (5) Ambiguities in the sequential assignments might occur if, for example, the four-bond polarization transfer from ^{15}N of Gly3 to ^{13}CO of Ala1 were more efficient than the two-bond transfer from ^{15}N of Gly3 to ^{13}CO of Gly3. This circumstance is rather unlikely because of the longer distance involved in a direct transfer from ^{15}N of Gly3 to ^{13}CO of Ala1, or the requirement for multiple intervening steps in an indirect transfer. One also expects cross-peaks from four-bond transfers to be weak in general because the spin polarization will tend to distribute itself among at least five nuclei.

As discussed above, the data in Figure 8 permit the assignment of all observed ^{13}CO and ^{15}N shifts to residue number but do not permit the unique assignment of all shifts to particular inequivalent AlaGlyGly molecules. Specifically, if the cross-peaks at (^{13}CO shift,^{15}N shift) = (159.2 ppm,77.4 ppm) and (201.9 ppm,77.4 ppm) are assigned to inequivalent molecule A and the cross-peaks at (168.6 ppm,108.8 ppm) and (207.8 ppm,108.8 ppm) are assigned to inequivalent molecule B, then either (i) the cross-peak at (187.2 ppm,194.5 ppm) belongs to molecule A and the cross-peak at (178.8 ppm,180.4 ppm) belongs to molecule B or (ii) the cross-peak at (187.2 ppm,194.5 ppm) belongs to molecule B and the cross-peak at (178.8 ppm,180.4 ppm) belongs to molecule A. Both possible assignments to inequivalent molecules were considered. Case (i) was found to give a smaller RMSD for ^{13}CO shifts and is reported in Table 2.

Table 3 displays the cross-peak intensities (i.e., volumes) extracted from Figure 6. One might expect that these intensities could be reproduced in numerical simulations of the nuclear spin quantum dynamics under the pulse sequence in Figure 7, using the known structure of AlaGlyGly and the crystal orientation in the magnetic field derived above. Accurate

(86) Tycko, R.; Weliky, D. P. *J. Chem. Phys.* **1996**, *105*, 7915−7930.
(87) Oas, T. G.; Hatzell, C. J.; McMahon, T. J.; Drobny, G. P.; Dahlquist, F. W. *J. Am. Chem. Soc.* **1987**, *109*, 5956−5962.
(88) Walling, A. E.; Pargas, R. E.; de Dios, A. C. *J. Phys. Chem. A* **1997**, *101*, 7299−7303.
(89) Wu, C. H.; Ramamoorthy, A.; Gierasch, L. M.; Opella, S. J. *J. Am. Chem. Soc.* **1995**, *117*, 6148−6149.
(90) Herzfeld, J.; Berger, A. E. *J. Chem. Phys.* **1980**, *73*, 6021−6030.

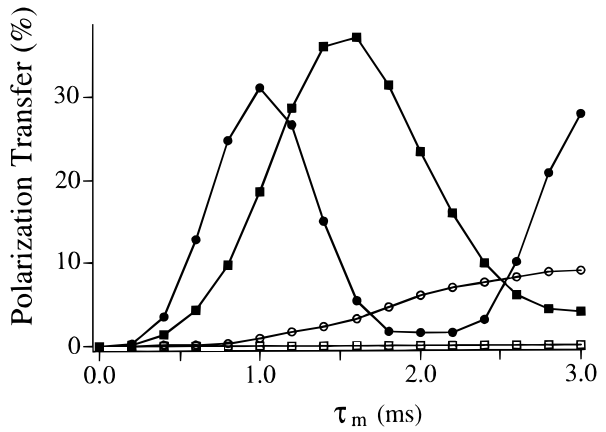

Figure 10. Simulation results for the resonance offset dependence of polarization transfer efficiency from ^{15}N to nonbonded ^{13}CO via through-bond dipolar interactions for a model three-spin system (^{15}N−^{13}C$_\alpha$−^{13}CO). Initial transverse magnetization was prepared only on ^{15}N and transferred to ^{13}C under WALTZ-5 CP sequences with rf amplitudes of 30 kHz for ^{15}N and ^{13}C spins. The rf fields are applied at the exact NMR frequencies of the ^{15}N and ^{13}CO nuclei. The dependence of the ^{13}CO NMR signals on the polarization transfer time (τ_m) is plotted for various resonance offsets of ^{13}C$_\alpha$ (●, 0 kHz; ■, −10 kHz; ○, −20 kHz; □, −30 kHz). Internuclear distances are 1.47 and 1.50 Å, for ^{15}N−^{13}C$_\alpha$ and^{13}C$_\alpha$−^{13}CO, respectively. The ^{15}N−^{13}C$_\alpha$−^{13}CO plane is taken to be perpendicular to the static magnetic field. In these simulations, the dipole−dipole coupling between the ^{15}N and ^{13}CO spins is not included, so only polarization transfer mediated by the intervening ^{13}C$_\alpha$ is observed.

simulations of this type are not possible, however, because the experimentally observed dependences of cross-peak intensities on τ_m are influenced by interactions that cannot feasibly be included in quantum dynamical simulations, principally residual couplings of ^{15}N and ^{13}C nuclei to numerous protons as well as spin relaxation processes and long-range couplings to other ^{15}N and ^{13}C nuclei. Quantum dynamical simulations can only be carried out for relatively small spin systems. As is well-known, simulations on small spin systems always lead to oscillatory dependences of the cross-peak intensities on polarization transfer times, as in Figure 10, rather than build-up rates, strongly damped oscillations, or asymptotic approaches to the steady state that are observed in polarization transfer experiments on real systems. The experimental cross-peak intensities are also affected by the efficiency of ^{1}H/^{15}N cross-polarization, which cannot be simulated because of its multispin nature. Nonetheless, numerical simulations are useful for assessing, in a qualitative manner, the effects of molecular orientation on the observability of the cross-peaks that are required for sequential assignments. We have carried out simulations of polarization transfer from amide ^{15}N nuclei to ^{13}CO nuclei for the five-spin system comprised of the backbone nuclei of AlaGlyGly from ^{13}C$_\alpha$ of Ala1 through ^{13}CO of Gly2 in a 9.39 T field, using the known molecular structure,[78,79] the CSA tensors described above, and the Hartmann−Hahn-matched WALTZ-5 sequence employed in our experiments. Results for selected magnetic field directions relative to the molecule are shown in Figure 11. These results illustrate the sensitivity of the one- and two-bond polarization transfers to the field direction, due primarily to the proportionality of the ^{15}N−^{13}C and ^{13}C−^{13}C dipole−dipole couplings to 3 $\cos^2\theta - 1$, where θ is the angle between the field and the internuclear vector. Particular couplings vanish at the magic angle, i.e., when $\theta = \cos^{-1} 1/\sqrt{3}$. Polarization transfer from ^{15}N of Gly2 to ^{13}CO of Ala1 is slowest when this peptide bond is exactly at the magic angle, suppressing direct one-bond

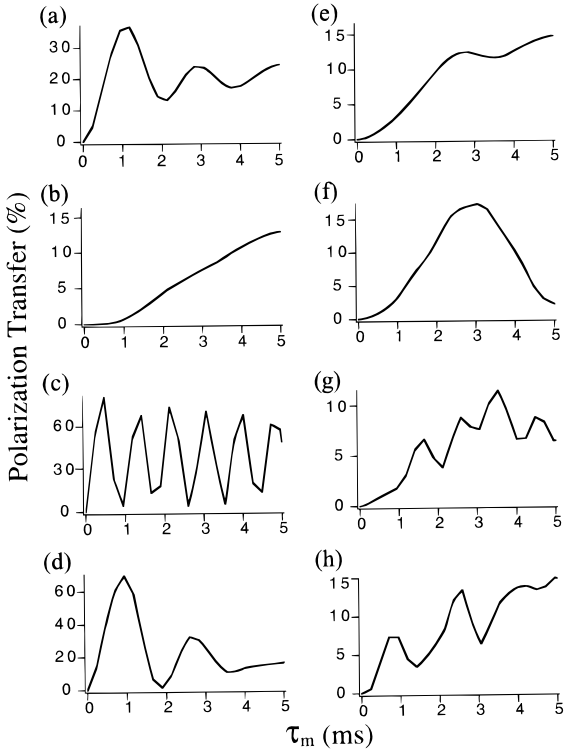

Figure 11. Numerical simulations of polarization transfer from ^{15}N to ^{13}CO for the five-spin system comprised of ^{13}C$_\alpha$ of Ala1 through ^{13}CO of Gly2 in AlaGlyGly at 9.39 T, for various directions of the magnetic field relative to the crystallographic unit cell, as specified by angles α and β (see text). Parts a−d are for one-bond polarization transfer from ^{15}N of Gly2 to ^{13}CO of Ala1. Parts e−h are for two-bond polarization transfer from ^{15}N of Gly2 to ^{13}CO of Gly2. The field direction is (α,β) = (120°,160°), (116.9°,29.7°), (41.3°,62.2°), and (286.4°,60.7°) in parts (a, e), (b, f), (c, g), and (d, h), respectively. These directions correspond respectively to the direction determined by fitting the experimental ^{13}CO chemical shifts (Figure 6 and Table 1), an orientation in which the bond between ^{15}N of Gly2 and ^{13}CO of Ala1 is at the magic angle, an orientation in which the bond between ^{15}N of Gly2 and ^{13}C$_\alpha$ of Gly2 is at the magic angle, and an orientation in which the internuclear vector between ^{15}N of Gly2 and ^{13}CO of Gly2 is at the magic angle. All dipole−dipole couplings and, hence, all possible polarization transfer pathways are included in these simulations.

transfer. (Figure 11b). However, the polarization transfer is not negligible, even in this least favorable cases, because of the availability of alternative polarization transfer pathways. Interestingly, polarization transfer from ^{15}N of Gly2 to ^{13}CO of Gly2 is relatively insensitive to the field direction, even when the internuclear vector from ^{15}N of Gly2 to ^{13}CO of Gly2 is exactly at the magic angle (Figure 11h), suppressing the direct two-bond transfer, and when the bond between ^{15}N of Gly2 and ^{13}C$_\alpha$ of Gly2 is exactly at the magic angle, suppressing two-bond transfer through the intervening ^{13}C$_\alpha$ (Figure 11g). The results in Figure 11 suggest that one-bond and two-bond cross-peaks should be observable for the vast majority of peptide backbone orientations, provided that the rf pulse sequence used for polarization transfer is sufficiently broadband, allowing multiple polarization transfer pathways. Sequential assignments do not depend on the one-bond cross-peaks being more intense than the two-bond cross-peaks.

Extension to Three-Dimensional Spectroscopy. The decoupling and polarization transfer methods described above can be readily extended to higher-dimensional spectroscopy in order to increase the resolution and structural information content of the measurements. As an example, Figure 12 shows the rf pulse

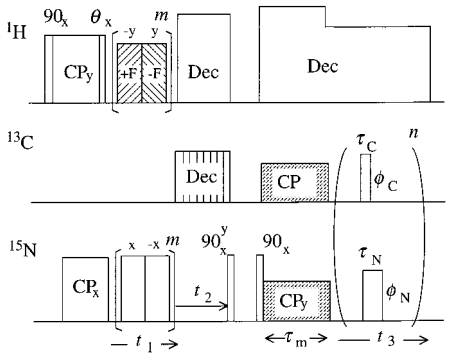

Figure 12. Rf pulse sequence for ^{13}C-detected three-dimensional spectroscopy correlating ^{1}H−^{15}N dipole−dipole couplings (t_1 dimension) with ^{15}N chemical shifts (t_2 dimension) and ^{13}CO shifts (t_3 dimension). ^{1}H−^{15}N couplings are recorded with a PISEMA sequence,[65,66] with +F and −F representing positive and negative resonance offsets for magic-angle irradiation and *m* representing the number of repetitions.

sequence for 3D spectroscopy in which the t_1 dimension records ^{1}H−^{15}N dipole−dipole couplings under a PISEMA sequence,[65,66] the t_2 dimension records ^{15}N chemical shifts, and the t_3 dimension records ^{13}CO shifts. Figure 13a shows the ^{15}N-detected 2D ^{1}H−^{15}N coupling/^{15}N shift PISEMA spectrum of the 33 mg uniformly ^{15}N- and ^{13}C-labeled AlaGlyGly crystal, obtained at 9.39 T. This spectrum was obtained as previously described,[65,66] but with time-shared ^{13}C TPPM decoupling during signal acquisition, and is included to display the ^{1}H−^{15}N dipolar splittings. Figure 13b shows 2D strips extracted from the full ^{13}C-detected 3D spectrum at frequencies in the ^{1}H−^{15}N dipolar dimension where signals are observed for the two magnetically inequivalent AlaGlyGly molecules. Full sequential assignment of the 3D signals for both molecules is possible as indicated. Note that, although the amino ^{15}N signals for the two molecules are not resolved in the 2D PISEMA spectrum, they are resolved in the 3D spectrum because of differences in the ^{13}CO chemical shifts of Ala1.

Discussion and Conclusions

The results presented above demonstrate the feasibility of obtaining resolved, ^{13}C-detected 1D and 2D chemical shift spectra of uniformly labeled, oriented peptides. A single 2D ^{15}N/^{13}C correlation spectrum provides spectral resolution, sequential assignments, and structural constraints in the form of anisotropic ^{15}N and ^{13}C chemical shifts. 3D spectra have even higher resolution and additional structural constraints in the form of ^{1}H−^{15}N dipole−dipole couplings. The success of these solid-state NMR experiments is dependent on several methodological innovations, including PSH ^{13}C decoupling to allow the detection of resolved ^{13}CO chemical shift spectra in the presence of strong dipole−dipole couplings to aliphatic ^{13}C nuclei, WALTZ-5 CP to provide efficient ^{15}N/^{13}C polarization transfer across the ^{13}CO spectral range, heteronuclear WALTZ-16 or TPPM ^{13}C−^{15}N decoupling to produce high resolution in the ^{15}N spectrum at high fields, and pulsed heteronuclear TPPM ^{15}N−^{13}C decoupling to remove heteronuclear dipolar splittings during the detection of ^{13}C NMR signals. To our knowledge, these decoupling and polarization transfer techniques have not been demonstrated previously, either separately or in combination.

Uniformly labeled AlaGlyGly single crystals were chosen as model systems for the development of the solid state NMR methods described above because they provide a simple and robust way to investigate the spectroscopic properties of peptide molecules that are oriented with respect to the static magnetic

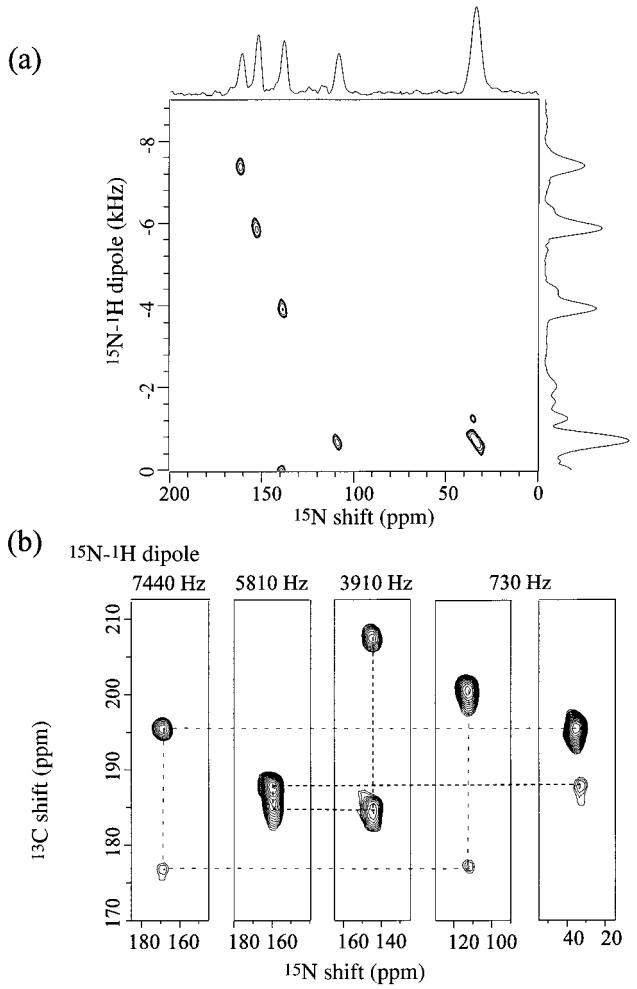

Figure 13. (a) Two-dimensional ^{15}N-detected PISEMA spectrum of a 33 mg crystal of uniformly ^{15}N- and ^{13}C-labeled AlaGlyGly (10% labeled molecules diluted in 90% unlabeled molecules), observed at 40.6 MHz (9.39 T field). During signal acquisition, heteronuclear ^{13}C−^{15}N decoupling was accomplished by time-shared TPPM decoupling, with 15 μs ^{13}C pulses separated by 5 μs delays and an rf amplitude of 33 kHz. The pulse phases alternated between +22.5° and −22.5°. Thirty-two t_1 points were acquired, with a 40 μs increment and eight scans for each t_1 point. In data processing, linear prediction was employed in the t_1 dimension to reduce truncation artifacts. (b) Two-dimensional strips extracted from the ^{13}C-detected three-dimensional spectrum obtained with the pulse sequence in Figure 11. ^{1}H-^{15}N dipolar frequencies are specified above each strip. Sequential assignments, progressing from the amino ^{15}N (^{15}N shifts near 35 ppm) to the carboxyl ^{13}CO, are indicated for each of the two magnetically inequivalent AlaGlyGly molecules. Experimental conditions were as in Figure 6, but with τ_m = 2.0 ms, ^{13}C rf carrier frequences at 120 ppm in t_2, 40 ppm in t_3, and 130 ppm during WALTZ CP, and the ^{15}N carrier frequency at 120 ppm during WALTZ CP. Eight t_1 points were acquired, with a 40 μs increment. Thirty-two t_2 points were acquired, with a 80 μs increment. Only a real component was acquired in t_1, and real and imaginary components were acquired in t_2, with 28 scans for each free induction decay. Linear prediction was employed in the t_1 dimension to reduce truncation artifacts.

field of the NMR spectrometer. In these model systems, the only unknown aspect of the structure was the direction of the magnetic field relative to the crystal unit cell. This field direction was determined by fitting to the experimental 2D spectrum. Six anisotropic ^{13}CO chemical shifts were fit with only two angular parameters. The good agreement between experimental and fitted chemical shifts, particularly for the ^{13}CO shifts but also for the ^{15}N shifts (see discussion above and Tables 1 and 2),

demonstrates the validity of the sequential resonance assignments and the accuracy of the structural information contained in the anisotropic chemical shifts. If the peptide backbone conformation were unknown, the conformation could be determined from or experimentally constrained by the assigned ^{15}N and ^{13}C shifts.[44,45,48,49,53,56−62,64−67]

Higher-dimensional spectroscopy, also using the homonuclear and heteronuclear decoupling techniques presented above, enhances the resolution and structural information content of solid state NMR measurements on uniformly labeled, oriented systems. Addition of a third dimension in which ^{1}H−^{15}N dipole−dipole couplings are recorded using a PISEMA sequence[65,66] is particularly valuable because the dispersion and resolution of signals under PISEMA has been shown to be high and the ^{1}H−^{15}N dipole−dipole couplings have a simple interpretation in terms of peptide plane orientation. Directly bonded ^{15}N−^{13}CO dipole−dipole couplings could also be measured in an additional frequency dimension.

Recent work by Opella and co-workers[72−74] has also demonstrated certain advantages of combined ^{15}N and ^{13}C labeling and triple-resonance solid-state NMR spectroscopy for resonance assignments and the extraction of structural constraints in studies of oriented peptides and proteins. In particular, Gu and Opella[73] have reported 2D ^{13}C/^{15}N chemical shift correlation spectra of a uniformly labeled *N*-acetyl glycine crystal and 3D ^{13}C shift/^{1}H−^{15}N coupling/^{15}N shift spectra of a selectively labeled *N*-acetyl glycine crystal. In these experiments, ^{13}C homonuclear decoupling is accomplished with a Lee-Goldburg sequence,[91] which is not compatible with ^{13}C detection. Thus, the directly detected signals are from ^{15}N nuclei. In contrast, the 2D spectra in Figures 6 and 8 above are ^{13}C-detected, as motivated by the generally higher sensitivity of ^{13}C-detected experiments. The spectra reported by Gu and Opella show good resolution and the potential for sequential assignments, but sequential assignments are not demonstrated experimentally because the model system is a derivatized amino acid (i.e., a monopeptide). Tan et al.[74] have reported a 2D ^{15}N/^{13}C chemical shift correlation spectrum of a specifically ^{15}N-Lys- and ^{13}CO−Phe-labeled, magnetically oriented fd bacteriophage. In this case, ^{13}C signals are directly detected but homonuclear decoupling is unnecessary because the sample is specifically labeled and therefore exhibits no strong ^{13}C−^{13}C couplings.

^{13}CO chemical shifts are especially useful as structural parameters for determination of a peptide backbone conformation because of the large ^{13}CO shift anisotropy and the well characterized and relatively constant orientation of the ^{13}CO CSA tensor relative to the peptide bond. For this reason, the methods described above focus on the resolution and detection of ^{13}CO signals. Although information in aliphatic ^{13}C NMR signals is lost in spectral dimensions that include PSH decoupling, such information could be recovered in additional dimensions. For example, $^{13}C_{\alpha}$−^{15}N dipole−dipole couplings, which would provide independent structural information and possibly additional sequential assignments, could be observed in an indirectly detected dimension that employs homonuclear ^{13}C decoupling (e.g., WAHUHA or Lee−Goldburg decoupling) but no heteronuclear ^{15}N−^{13}C decoupling. Side-chain ^{13}C chemical shifts could be observed in an indirectly detected dimension that employs homonuclear ^{13}C decoupling. Side chain ^{1}H−^{13}C dipole−dipole couplings could be observed in a dimension that employs a ^{1}H/^{13}C PISEMA sequence. These anisotropic chemical shifts and couplings would provide information about side chain conformations. Proteins comprised of α-helices parallel to the magnetic field exhibit limited frequency dispersion of backbone NMR signals, because of the very similar orientation of all peptide planes with respect to the field. In such cases, observation of NMR frequencies associated with side chains may significantly increase the resolution of multidimensional spectra. A key issue that remains to be addressed regarding side chain signals is the efficiency of spin polarization transfers among backbone and side chain nuclei, which will determine the sensitivity of such experiments.

What are the prospects for successful application of these techniques to bona fide proteins, for example in mechanically or magnetically oriented phospholipid bilayers? The critical considerations are resolution and sensitivity. The 2D spectra in Figures 6 and 8 show that six inequivalent residues are quite easily resolved. With line widths similar to those in Figures 6 and 8 (which requires that variations in the protein orientation relative to the magnetic field be on the order of 2° or less), and with ^{13}CO and ^{15}N chemical shift ranges of approximately 80 ppm (reduced by the nonlinear scaling discussed above) and 170 ppm, it would be possible to resolve on the order of 100 cross-peaks, as a conservative estimate. With addition of a third, independent spectral dimension, signals from more than 100 residues could be resolved. Sequential assignment of the cross-peaks requires the detection of cross-peaks that connect ^{15}N and ^{13}CO nuclei separated by two bonds. As discussed above, improvements in the bandwidth of ^{15}N/^{13}C cross-polarization sequences are required for all two-bond cross-peaks to be observable in a single spectrum, especially at very high fields. With improved sequences, or with the acquisition of several independent spectra using different cross-polarization times and rf carrier frequencies, a majority of the cross-peaks could be in sequentially assignable stretches. The sensitivity of the 2D measurements in Figures 6 and 8 is currently such that at least one micromole of uniformly labeled peptide or protein is required. Specifically, the AlaGlyGly crystal used for Figure 8a,b contained 1.3 μmol of each inequivalent site, and these 2D spectra were acquired with a home-built NMR probe in 13 and 32 h, respectively. Improvements in probe efficiency and polarization transfer efficiency, reductions in the dead time and noise figure of the receiver circuitry of the NMR spectrometer, and lower temperatures could improve the sensitivity significantly. Hence, it appears that applications to bona fide proteins are well within the realm of possibility.

Acknowledgment. We are grateful to Prof. A. Ramamoorthy for useful discussions and kind instruction on growth of a single crystal. We thank Prof. O. N. Antzukin for kindly helping us to analyze the spinning sideband pattern of ^{15}N-labeled AlaGlyGly and Prof. A. C. deDios for providing unpublished data on chemical shift tensors used in simulations (not shown) that helped guide the development of homonuclear decoupling sequences. Y.I. thanks the Japan Society for the Promotion of Science for a postdoctoral research fellowship at the NIH. This work was supported in part by the NIH Intramural AIDS Targeted Antiviral Program.

Appendix

Theoretical Analysis of Phase-Modulated Selective ^{13}C Decoupling. To clarify the advantage of phase-modulated selective decoupling over unmodulated selective decoupling, it is useful first to discuss unmodulated decoupling. Consider a system of two ^{13}C spins coupled by dipole−dipole and scalar couplings under weak pulsed rf irradiation. The spin Hamiltonian may be written as

(91) Lee, M.; Goldberg, W. I. *Phys. Rev.* **1965**, *140*, A1261−1271.

$$H(t) = H_{CSA} + H_{rf}(t) + H_{IS} \quad \text{(A-1)}$$

with

$$H_{CSA} = \omega_S S_z + \omega_I I_z \quad \text{(A-2)}$$

$$H_{rf}(t) = \omega_I(t)(S_x + I_x) \quad \text{(A-3)}$$

$$H_{IS} = D_{IS}(3I_zS_z - \mathbf{I}\cdot\mathbf{S})/2 + J_{IS}\mathbf{I}\cdot\mathbf{S} \quad \text{(A-4)}$$

where **S** and **I** are the angular momentum vector operators, the rf amplitude $\omega_1(t)$ equals ω_C during the selective decoupling pulses and zero between the pulses, ω_S and ω_I are the resonance offsets from the rf carrier for spins *S* and *I*, and D_{IS} and J_{IS} are the dipole−dipole and scalar coupling constants. We are interested in determining the resonance offset (i.e., the chemical shift) of spin *S* while decoupling it from spin *I*. We consider the case in which $0 < \omega_c\tau_c \ll \pi$ and $0 < \omega_I\tau \ll \omega_c\tau_c \ll \omega_S\tau, \omega_c\tau$, i.e., the case of a train of short pulses with small flip angles applied almost on resonance with spin *I* but far off resonance with spin *S*. In addition, we assume that the average rf field $\omega_{av} = \omega_c\tau_c/\tau$ satisfies $\omega_{av} > |D_{IS}|, |J_{IS}|$, since this is necessary for effective decoupling. In this case, we can approximate the rf pulse train by a cw rf field with amplitude ω_{av}. To estimate the line width due to residual dipole−dipole couplings, we transform the system into an interaction representation with respect to $H_{rf}(t) + H_{CSA}$ and calculate the average of the time-dependent dipole−dipole and scalar couplings $\bar{H}_{eff}$ in this representation. The resulting effective coupling Hamiltonian can be expressed as

$$\bar{H}_{eff} = \{(D_{IS} + J_{IS}) \cos\theta_I \cos\theta_S + (-D_{IS}/2 + J_{IS}) \sin\theta_I \sin\theta_S\}\tilde{I}_Z\tilde{S}_Z \quad \text{(A-5)}$$

with

$$\tilde{I}_Z = I_z \cos\theta_I + I_x \sin\theta_I \quad \text{(A-6a)}$$

$$\tilde{S}_Z = S_z \cos\theta_S + S_x \sin\theta_S \quad \text{(A-6b)}$$

and

$$\tan\theta_k = \omega_{av}/\omega_k \quad \text{(A-7)}$$

where $k = I$ or *S*. Complete removal of dipole−dipole and scalar couplings is accomplished only for an ideal selective decoupling condition $\theta_I = \pi/2$ and $\theta_S = 0$. However, it is difficult to achieve or approximate this ideal condition for all the residues in peptides or proteins because $^{13}C_\alpha$ and $^{13}C_\beta$ spins have CSA and isotropic chemical shift differences that are not negligible. For example, when $\omega_{av}/2\pi = 10$ kHz, $\omega_I/2\pi = 1$ kHz, and $\omega_S/2\pi = 20$ kHz, the dipolar scaling factor is $\cos\theta_I \cos\theta_S - {}^1/_2 \sin\theta_I \sin\theta_S = -0.13$. Consequently, considerable line broadening due to the residual dipole−dipole couplings is expected in the spectrum obtained by selective decoupling without phase modulation.

Further narrowing can be accomplished by second averaging[92] with phase-modulated selective decoupling. To produce an extra selective decoupling rf field after the first average, we adopt the two-phase modulation used in TPPM decoupling[77] developed for broadband ^{1}H decoupling in solids, although more sophisticated designs of phase and amplitude modulations[93] might produce better results. In the two-phase modulation scheme, the rf decoupling field is described by

$$H_{rf}(t) = H_x(t) + H_y(t) \quad \text{(A-8)}$$

$$H_x(t) = \omega_I(t) \cos\phi(t)(I_x + S_x) \quad \text{(A-9)}$$

$$H_y(t) = \omega_I(t) \sin\phi(t)(I_y + S_y) \quad \text{(A-10)}$$

where $\phi(t)$ switches between $+\phi$ and $-\phi$ after each group of *N* successive τ intervals. To generate the second decoupling field after the first averaging, the condition $N\omega_C\tau_C \approx \pi$ must be satisfied so that the phase modulation resonates with the first decoupling field. Also, ϕ should be small enough that $H_y(t)$ can be considered as a perturbation with respect to $H_x(t)$. Under this condition, we transform the system into an interaction representation with respect to $H_x(t) + H_{CSA}$ and obtain the effective Hamiltonian

$$H_{eff} = \tilde{H}_{rf} + \{(D_{IS} + J_{IS}) \cos\theta_I \cos\theta_S + (-D_{IS}/2 + J_{IS}) \sin\theta_I \sin\theta_S\}\tilde{I}_Z\tilde{S}_Z \quad \text{(A-11)}$$

with

$$\tilde{H}_{eff} = (\omega_{av} \sin\phi/\pi)I_y \quad \text{(A-12)}$$

It is important to note that the second decoupling field described by $\tilde{H}_{rf}$ is not generated for the observed spin *S* although the phase modulated rf field is also applied to *S* spin. This is because the effective field $(\omega_{av}^2 + \omega_S^2)^{1/2}$ is far from synchronization with the phase modulation rate ω_{av} for large offsets ω_S. Thus, the decoupling field generated by second averaging is also selectively applied to the *I* spin. The second selective decoupling field $\tilde{H}_{rf}$ is applied along the *y*-axis, which is perpendicular to the tilted quantum axis $\tilde{I}_z$. Hence, all the residual dipole−dipole and scalar couplings are simply removed by $\tilde{H}_{rf}$, as in heteronuclear decoupling.

JA9915753

(92) Pines, A.; Waugh, J. S. *J. Magn. Reson.* **1972**, *8*, 354−365.
(93) Ishii, Y.; Terao, T. *J. Chem. Phys.* **1998**, *109*, 1366−1374.